A LETTERS JOURNAL EXPLORING
THE FRONTIERS OF PHYSICS

May 2022

EPL, **138** (2022) 41001
doi: 10.1209/0295-5075/ac6e4b

www.epljournal.org

Polar flocks with discretized directions: The active clock model approaching the Vicsek model

SWARNAJIT CHATTERJEE[1(a)], MATTHIEU MANGEAT[1(b)] and HEIKO RIEGER[1,2(c)]

[1] *Center for Biophysics & Department for Theoretical Physics, Saarland University - D-66123 Saarbrücken, Germany*
[2] *INM Leibniz Institute for New Materials - Campus D2 2, 66123 Saarbrücken, Germany*

received 2 March 2022; accepted in final form 10 May 2022
published online 8 June 2022

Abstract – We consider the off-lattice two-dimensional q-state active clock model (ACM) as a natural discretization of the Vicsek model (VM) describing flocking. The ACM consists of particles able to move in the plane in a discrete set of q equidistant angular directions, as in the active Potts model (APM), with an alignment interaction inspired by the ferromagnetic equilibrium clock model. We find that for a small number of directions, the flocking transition of the ACM has the same phenomenology as the APM, including macrophase separation and reorientation transition. For a larger number of directions, the flocking transition in the ACM becomes equivalent to the one of the VM and displays microphase separation and only transverse bands, *i.e.*, no re-orientation transition. Concomitantly also the transition of the $q \to \infty$ limit of the ACM, the active XY model (AXYM), is in the same universality class as the VM. We also construct a coarse-grained hydrodynamic description for the ACM and AXYM akin to the VM.

Active matter consists of particles that consume energy and convert it, for instance, into directed motion. Being manifestly out of equilibrium active matter systems display novel many-particle effects or collective phenomena, like flocking, motility-induced phase separation, giant number fluctuations, active turbulence, etc. New models have been developed in the last two decades to understand and unravel the physical principles governing active matter systems [1]. The paradigmatic model for collective motion of animal groups, like bird flocks, buffalo herds, fish schools, is the Vicsek model (VM) [2], in which particles moving with constant velocity align their direction of motion with the average direction of their neighbors. At low noise and large density the VM displays a flocking transition to collective motion in a common direction. Subsequent studies showed that the way in which noise and disorder are introduced into the system [3,4], the range and type of the interactions [5–8] and alignment rules [9,10] influence the characteristics of pattern formation and the type of phase transition occurring in Vicsek-like models.

Even the nature of the flocking transition of the original VM was debated for a long time: originally thought to be continuous [2] recent studies showed that it is discontinuous, reminiscent of a liquid-gas transition rather than an order-disorder transition [11]. In contrast to conventional first-order phase transition scenarios, in which the system phase-separates macroscopically into a liquid and a gas phase in the coexistence region, the VM microphase separates into liquid bands of finite width moving coherently through the gas phase due to giant density fluctuations that break large liquid domains and arrest band coarsening [11]. Remarkably, such a microphase separation is absent in discretized versions of flocking models: the active Ising model (AIM) [12], the q-state active Potts model (APM) [13], and an earlier version of the APM with volume exclusion effects [5] which shows a surprisingly rich variety of self-organized patterns, all manifest macrophase separation in the coexistence region with only one liquid band moving in a gas background in a large aspect ratio rectangular geometry. In contrast to the VM, the APM displays additionally a reorientation transition from transversally moving bands for low particle velocities to longitudinally moving bands for high particles velocities [13].

A natural discretization of the VM (in 2d) is the 2d q-state active clock model (ACM), consisting of particles able to move in the plane in a discrete set of q equidistant angular directions, as in the AIM or APM, with an alignment interaction inspired by the ferromagnetic equilibrium

(a)E-mail: swarnajitchatterjee@gmail.com (corresponding author)
(b)E-mail: mangeat@lusi.uni-sb.de
(c)E-mail: heiko.rieger@uni-saarland.de

clock model [14], approaching the ferromagnetic XY model in the limit $q \to \infty$ [15]. Three questions arise in this context: 1) What is the nature of a putative flocking transition in the ACM for different values of the number of states q, regarding the fact that the equilibrium clock model has continuous BKT transition at a temperature $T_{\rm BKT}$ into a quasi-long–range ordered phase and for $q > 4$ another transition at a temperature $T_{\rm LRO} < T_{\rm BKT}$ into a long-range ordered phase [16]? 2) If the transition is first order, what are the characteristics of the coexistence region: microphase separation as in the VM or macrophase separation as in the AIM and APM? Do longitudinally moving bands exist? 3) Is the $q \to \infty$ limit of the ACM, the active XY model (AXYM), equivalent to the VM or does it remain macrophase separating as for finite q?

In this letter we will answer these question and will show that for a small number of states, the flocking transition of the ACM has the same phenomenology as the APM [13], including macrophase separation and reorientation transition. For a larger number of states, the flocking transition in the ACM becomes equivalent to the one of the VM and displays microphase separation and only transverse bands, *i.e.*, no re-orientation transition. Concomitantly also the transition of the AXYM is in the same universality class as the one of the VM. The letter is organized as follows: first we define the ACM in detail, then we present our numerical results and our hydrodynamic theory, and finally we discuss the implication of our findings.

Model. – The 2d q-state ACM consists of N particles moving in an off-lattice rectangular domain of size $L_x \times L_y$ with periodic boundary conditions and with average particle density $\rho_0 = N/L_xL_y$. Since no mutual exclusion among the particles is considered, ρ_0 can assume values larger than 1. Each particle carries a clock degree of freedom or angle $\theta \in \{0, 2\pi/q, 4\pi/q, \ldots, 2(q-1)\pi/q\}$, which also defines its preferred direction of motion in a biased diffusion. It can either jump to a new position or flip its angle. The hopping rate of a particle in state θ in the (discrete) direction ϕ is $W_{\rm hop} = D[1-\varepsilon/(q-1)]$ for $\phi \neq \theta$ and $W_{\rm hop} = D(1+\varepsilon)$ for $\phi = \theta$, where $D > 0$ is the diffusion constant and $\varepsilon \in [0, q-1]$ is the bias, or "velocity". Note that the total hopping rate is $W_{\rm hop}^{\rm tot} = qD$ and that $\varepsilon = 0$ corresponds to unbiased diffusion and $\varepsilon = q-1$ to ballistic motion in the direction of the clock angle. If the hopping angle is ϕ and we denote the position of the i-th particle at time t by $\mathbf{x}_i(t)$, then its position in the next time step is $\mathbf{x}_i(t) + \mathbf{e}_\phi$, where $\mathbf{e}_\phi$ is the unit vector in the ϕ-direction. The flipping rate from $\theta_i = \theta$ to $\theta_i = \theta'$ is derived via detailed balance from a local clock Hamiltonian

$$H_i = -\frac{J}{2\rho_i} \sum_{k\neq l, k,l \in \mathcal{N}_i} \cos(\theta_k - \theta_l), \qquad (1)$$

where J is the ferromagnetic coupling constant and ρ_i is the number of particles within its neighborhood $\mathcal{N}_i = \{j \text{ with } |\mathbf{x}_i - \mathbf{x}_j| \leqslant 1\}$:

$$W_{\rm flip} = \gamma \exp\left\{ \frac{\beta J}{\rho_i} \left[\mathbf{m}_i \cdot (\mathbf{e}_{\theta'} - \mathbf{e}_\theta) + 1 - \cos(\theta - \theta')\right] \right\}, \qquad (2)$$

where $\mathbf{m}_i = \sum_{j\in\mathcal{N}_i} (\cos\theta_j, \sin\theta_j)$ is the local magnetization and γ is a constant. The origin of the term $1 - \cos(\theta-\theta')$ in eq. (2) is the absence of self-interaction in the clock Hamiltonian in eq. (1) (see the Supplementary Material `Supplementarymeterial.pdf` (SM) for a detailed explanation). Although phenomenologically ACM is very similar to the APM [13], the Kronecker delta "Potts" interaction in the APM has been replaced by the cosine "clock" interaction in the ACM motivated by the $q \to \infty$ limit and whether one recovers the VM in that limit and here the ACM is clearly better suited than the APM.

For $q = 4$ and 6, one can define the ACM on square and triangular lattices, respectively, and identify the q different directions of motion to the q nearest neighbors. We analyzed these lattice versions, too, and obtained qualitatively identical results as those reported below, see the SM, but here we restrict ourselves to the off-lattice version which allows a straightforward $q \to \infty$ limit (AXYM) and is also closer to the original VM. In the limit $q \to \infty$ the rescaled quantities $\overline{D} = qD$ and $\overline{\varepsilon} = \varepsilon/(q-1)$ have to stay finite and the angles become continuous with $\theta \in [0, 2\pi]$. The jump rate of a particle in state θ in the (continuous) direction ϕ becomes $W_{\rm hop} = \overline{D}(1 - \overline{\varepsilon})$ for $\phi \in [0, 2\pi]$ and $W_{\rm hop} = \overline{D}\overline{\varepsilon}$ for $\phi = \theta$.

We performed Monte Carlo simulations of the q-state ACM and the AXYM, which evolve in discrete time steps of length Δt. In each time-step N (=number of particles) single particle updates are performed, one of which consists in choosing randomly a particle which then either updates its spin state to $\theta' \neq \theta$ chosen randomly with probability $p_{\rm flip} = W_{\rm flip}\Delta t$, or hops to one of the q directions with probability $p_{\rm hop} = \overline{D}\Delta t$: in a random direction with probability $(1-\overline{\varepsilon})p_{\rm hop}$ or in the direction θ with probability $\overline{\varepsilon}p_{\rm hop}$. The probability that nothing happens during this single particle update is $p_{\rm wait} = 1 - p_{\rm flip} - p_{\rm hop}$. An expression for Δt can be chosen to minimize $p_{\rm wait}$: $\Delta t = [\overline{D} + \exp(2\beta J)]^{-1}$. This is a hybrid dynamics combining Monte Carlo and a real-time dynamics previously used in the simulations of the AIM [12] and the APM [13]. Without any loss of generality, we can take $\overline{D} = 1$, $J = 1$ and $\gamma = 1$.

We consider mainly a rectangular domain with a large aspect ratio with $L_x = 400$ and $L_y = 50$ for the computation of the phase diagram and other quantities. $L_x = 800$ with varying L_y are considered for the snapshots presented. Simulations are performed for three control parameters: the noise is regulated by $\beta = 1/T$, $\rho_0 = N/L_xL_y$ defines the average particle density, and $\overline{\varepsilon}$, the self-propulsion parameter, dictates the effective velocity of the particles. The initial homogeneous system is prepared by assigning random initial position (x_i, y_i) and orientation θ_i to each particle and then we let the system evolve

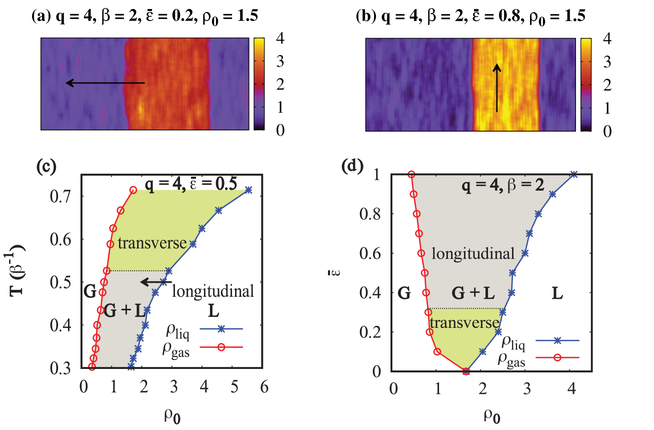

Fig. 1: (a), (b): stationary density profiles for $q = 4$, $\beta = 2$ and $\rho_0 = 1.5$ in a 400×50 domain showing the bulk phase-separation and reorientation transition from (a) transverse band motion for $\bar{\varepsilon} = 0.2$ to (b) longitudinal band motion for $\bar{\varepsilon} = 0.8$. The colorbar represents the particle density. (c) Temperature-density (T-ρ_0) phase diagram for $\bar{\varepsilon} = 0.5$, and (d) velocity-density ($\bar{\varepsilon}$-ρ_0) phase diagram for $\beta = 2$ of the $q = 4$-state ACM. The reorientation transition happens at $\beta = 1.9$ and $\bar{\varepsilon} = 0.32$, respectively.

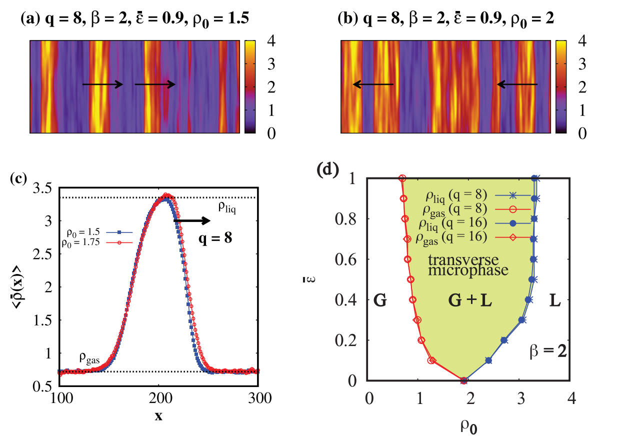

Fig. 2: (a), (b): stationary density profiles for the $q = 8$-state ACM, $\beta = 2$ and $\bar{\varepsilon} = 0.9$ in a 800×20 domain showing transversely moving microphase-separated bands for (a) $\rho_0 = 1.5$ and (b) $\rho_0 = 2$. The colorbar represents the particle density. (c) Time-averaged density profiles for $\rho_0 \in \{1.5, 1.75\}$ defining the two binodals ρ_{liq} and ρ_{gas}. (d) Velocity-density ($\bar{\varepsilon}$-ρ_0) phase diagrams for $q = 8$ and $q = 16$-state ACM obtained for $\beta = 2$ showing only transverse band motion.

under various control parameters for $t_{\text{eq}} = 10^5 \Delta t$ to reach the steady state. Following this, measurements are carried out with a maximum simulation time $t_{\max} = 20 t_{\text{eq}}$.

Phase diagrams and coexistence region. – In fig. 1(a) and fig. 1(b), we show stationary density profiles for the $q = 4$-state ACM on a 400×50 rectangular domain for fixed $\beta = 2$ and $\rho_0 = 1.5$ but for different bias: (a) $\bar{\varepsilon} = 0.2$ and (b) $\bar{\varepsilon} = 0.8$. As observed before in the VM [2,11], the AIM [12], and the q-state APM [13], the transition from a homogeneous gas phase to a polar liquid phase occurs through a liquid-gas coexistence phase, where a single band of polar liquid propagates on a disordered gaseous background. Akin to the 4-state APM [13], the band moves (a) transversally at small bias (velocity) $\bar{\varepsilon} = 0.2$ and (b) longitudinal with respect to the band direction at larger bias $\bar{\varepsilon} = 0.8$. The coexistence phase in both figures shows a fully phase-separated density profile with a single *macroscopic* liquid domain as observed previously in the context of lattice flocking models [12,13]. In fig. 1(c) and fig. 1(d), we display the temperature-density (T-ρ_0) phase diagram for $\bar{\varepsilon} = 0.5$ and the velocity-density ($\bar{\varepsilon}$-ρ_0) phase diagram for $\beta = 2$, respectively. The liquid and gas binodals ρ_{liq} and ρ_{gas}, which segregate the gas-liquid (G + L) coexistence phase from the two homogeneous phases, liquid (L) and gas (G), are extracted from the time-averaged phase-separated density profiles. Reported for the first time in the context of the APM [13], we observe a similar reorientation transition of the coexistence phase from transverse band motion at low velocities and high temperatures to longitudinal lane formation at high velocities and low temperatures for $q = 4$. The physical origin of this reorientation transition, as argued in ref. [13] with equivalent hopping rules, is the decrease of the transverse diffusion constant for large velocities, stabilizing the longitudinal lane formation. The reorientation transition occurs at $\beta = 1.9$ (c) and $\bar{\varepsilon} = 0.32$ (d), where the black dotted lines delimit the two co-existing phase domains which are further marked by two distinct colors: grey for longitudinal lane motion and yellow for transverse band motion. We have obtained similar results from the numerical simulations of the 4-state ACM on a square lattice (see the SM).

In fig. 2(a) and fig. 2(b), we show stationary density profiles for the $q = 8$-state ACM on a 800×20 rectangular domain for $\beta = 2$, $\bar{\varepsilon} = 0.9$ and (a) $\rho_0 = 1.5$ and (b) $\rho_0 = 2$. A *microphase* separation of the coexistence region, where periodically arranged ordered liquid bands move in the same direction in a gaseous background, is observed. The microphase-separated traveling bands are transverse in nature as observed first in the VM [2]. In a *microphase* separation, the traveling bands are not fully phase-separated and as established in ref. [11], one crucial characteristic of this *microphase* separation is that the band number n_b increases with the density ρ_0 as observed in figs. 2(a), (b). Time-averaged density profiles of the liquid-gas coexistence phase are shown in fig. 2(c) which suggest that the width of the polar liquid band does not increase significantly with the average density ρ_0 (see the SM for the algorithm which has been used to obtain the time-averaged profiles). It is well known that the band width does not affect the liquid (ρ_{liq}) and the gas (ρ_{gas}) binodals and we use this property to extract the relevant phase diagrams. In fig. 2(d), we represent the velocity-density ($\bar{\varepsilon}$-ρ_0) phase diagrams for $\beta = 2$ and for $q = 8$ and $q = 16$-state ACM. The two diagrams are very similar

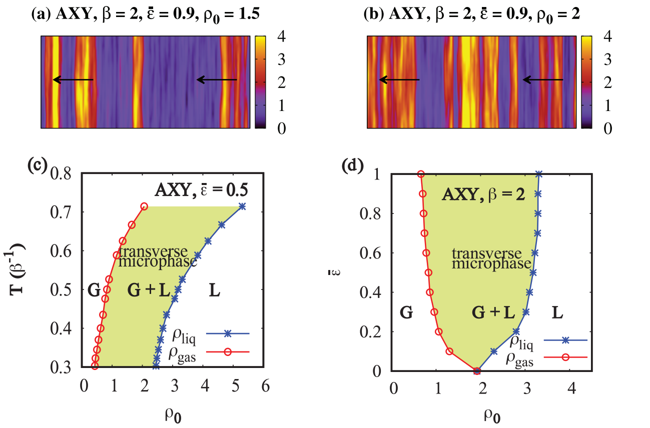

Fig. 3: (a), (b): stationary density profiles for the AXYM, $\beta = 2$ and $\bar{\varepsilon} = 0.9$ in a 800×20 domain showing transversely moving microphase-separated bands for (a) $\rho_0 = 1.5$ and (b) $\rho_0 = 2$. The colorbar represents the particle density. (c) Temperature-density (T-ρ_0) phase diagram for $\bar{\varepsilon} = 0.5$, and (d) velocity-density ($\bar{\varepsilon}$-ρ_0) phase diagram for $\beta = 2$ for the AXYM showing only transverse band motion.

both qualitatively and quantitatively and implying a similar physical picture of the q-state ACM for $q \geqslant 8$. The corresponding coexistence domain of the $q = 8$ and 16-state ACM is completely described by transversely traveling *microphase* separated bands. Although a reorientation transition occurs for $q = 6$-state ACM when simulated on a triangular lattice (see the SM), we do not observe any reorientation transition for off-lattice simulations for $q \geqslant 6$ at large bias $\bar{\varepsilon}$ as observed for $q = 4$.

In fig. 3(a) and fig. 3(b), we present the stationary density profiles in the coexistence phase of the AXYM (*i.e.*, for $q = \infty$) on a 800×20 rectangular domain and for $\beta = 2$, $\bar{\varepsilon} = 0.9$ and (a) $\rho_0 = 1.5$ and (b) $\rho_0 = 2$. The AXYM and VM possess the same $O(2)$ rotational symmetry but differ in their flipping and hopping rules. Nevertheless, we observe a *microphase* separation in the coexistence regime like in the VM [11] where the traveling bands are moving in the same direction and n_b is increasing with ρ_0. The temperature-density (T-ρ_0) and the velocity-density ($\bar{\varepsilon}$-ρ_0) phase diagrams are shown in fig. 3(c) for $\bar{\varepsilon} = 0.5$ and fig. 3(d) for $\beta = 2$, respectively. We do not observe the reorientation transition akin to the observation made for $q = 8$- and $q = 16$-state ACM. The velocity-density ($\bar{\varepsilon}$-ρ_0) phase diagram is also identical to fig. 2(d) both qualitatively and quantitatively and thus minimizing the statistical errors in the calculations of the binodals, these three diagrams can be merged in a single diagram which signifies that the system behaves similarly for large number of directions or large q-values. Moreover, for the q-state ACM and the AXYM we recover the characteristic velocity-density ($\bar{\varepsilon}$-ρ_0) phase diagram observed in other discrete flocking models [12,13]. However, the nature of the $\bar{\varepsilon} \to 0$ transition of the AXYM is different from the VM. The density at which the gas and liquid binodals

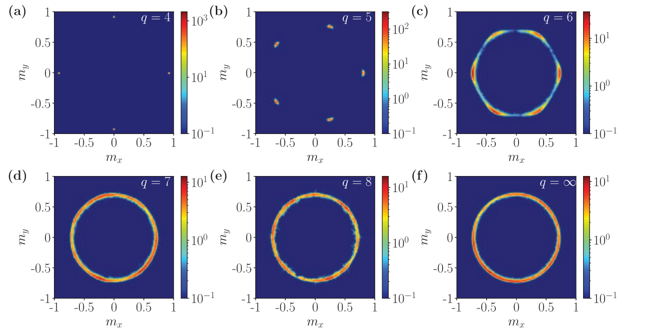

Fig. 4: Zero-activity limit of the order parameter distributions of the q-state ACM and AXYM ($q \to \infty$) in the liquid phase. Parameters: $L = 50$, $\beta = 2$, $\bar{\varepsilon} = 0$, and $\rho_0 = 3$.

intersect at $\bar{\varepsilon} = 0$ is finite ($\rho^* = 1.95$) for the AXYM whereas it is infinite for the VM, as argued in [11].

Zero activity limit ($\bar{\varepsilon} = 0$). – This limit is denoted as the Brownian clock model, reminiscent of the Brownian Potts model studied in [17]. We observe an order-disorder phase transition without a coexistence region, as observed for the AIM [12] and the APM [13]. In fig. 4, we show the distribution of the order parameter $\mathbf{m} = (m_x, m_y)$ with $m_x = \sum_{i=1}^{N} \cos\theta_i$ and $m_y = \sum_{i=1}^{N} \sin\theta_i$ in the ordered phase for $\beta = 2$, $\bar{\varepsilon} = 0$, and $\rho_0 = 3$ simulated on a square domain of system size $L = 50$ and averaged over time and several initial configurations. In fig. 4(a) and (b), we observe a well-defined long-range ordered phase (LRO) for $q = 4$ and $q = 5$, respectively, where the distributions manifest q isolated spots (pinned orientations) corresponding to the q-fold degeneracy of the ordered liquid phase with equal probability. In fig. 4(c)–(f), one observes for $q \geqslant 6$, ring-like distributions (unpinned orientations) signifying the Kosterlitz-Thouless (KT) type phase or the quasi-long–range ordered (QLRO) phase, where spin waves and vortices arrange the spin vectors. For discrete q-values, a LRO phase can be observed at large densities (see the SM) or small temperatures, which is not the case for the AXYM.

In the AXYM, particles can diffuse along any random direction with hopping rate $\bar{D}$, whereas the VM reduces to the two-dimensional XY model at the zero velocity limit (with immobile particles). Although it has been shown for the Brownian Potts model [17] that diffusion can change the nature of transition, the diffusive motion of the particles in the AXYM do not change the structure of the corresponding field theory compared to non-motile particles in the VM. Therefore, the Mermin-Wagner theorem is still applicable even though this system is driven out of equilibrium and the ordered phase we observe is QLRO in nature, akin to the XY model in two dimensions. The problem of diffusively moving spins, along with similar arguments, has also been studied explicitly in ref. [18] in the context of active phase oscillators with $O(2)$ symmetry, where QLRO is reported for normal diffusion of oscillators,

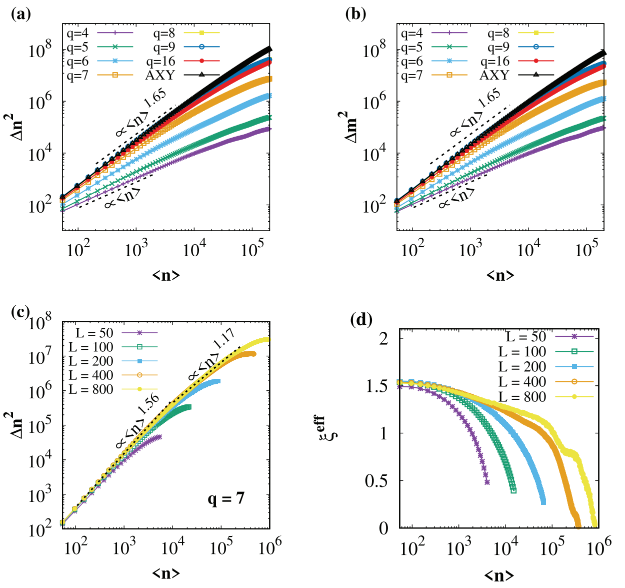

Fig. 5: (a), (b): number fluctuations $\Delta n^2 = \langle n^2\rangle - \langle n\rangle^2$ and magnetization fluctuations $\Delta m^2 = \langle m^2\rangle - \langle m\rangle^2$ *vs.* average particle number $\langle n\rangle$ for several q-values in a 400×400 domain. (c) Number fluctuations Δn^2 *vs.* $\langle n\rangle$ as a function of various system sizes for $q = 7$. (d) Effective exponent $\xi^{\rm eff}$ for the data plotted in (c). Parameters: $\beta = 2$, $\bar\varepsilon = 0.9$, and $\rho_0 = 6$.

whereas super-diffusive motion is needed in order to obtain long-range order in two dimensions.

Number fluctuations. – In fig. 5(a), (b), we show respectively the number fluctuations $\Delta n^2 = \langle n^2\rangle - \langle n\rangle^2$ and the magnetization fluctuations $\Delta m^2 = \langle m^2\rangle - \langle m\rangle^2$ for various q-values against the average particle number $\langle n\rangle$. n and m are respectively the number of particles and the magnetization in boxes of different sizes ℓ included in a 400×400 domain (with $\ell \leqslant 200$), with $\langle n\rangle = \rho_0\ell^2$. The data are for the liquid phase where $\beta = 2$, $\bar\varepsilon = 0.9$, and $\rho_0 = 6$. As shown in table 1, both the fluctuations behave like $\langle n\rangle^\xi$ with the fluctuation exponent $\xi \simeq \xi_n \simeq \xi_m$ increasing with q, from $\xi \simeq 1$ for $q = 4$ to $\xi \simeq 1.65$ for large q (and it saturates for $q \geqslant 8$). Consequently the number and magnetization fluctuations show a transition from uniform fluctuations for small q to giant fluctuations at larger q as they have been observed in the VM [11]. Although the existence of giant number fluctuations (GNF) were shown in Vicsek-like self-propelled particle models [6,7], the connection between GNF and micro-/macrophase separation was first hypothesized in ref. [11] in the context of VM where it has been argued that GNF ($\xi_n \simeq 1.6$) break large bulk liquid domains and consequently produce smectic-like microphase state in the coexistence regime whereas the system undergoes bulk phase separation when the density fluctuations are normal ($\xi_n \simeq 1$) [12]. In the ACM, therefore, these GNF for large q might be responsible for the microphase separation in the coexistence regime as shown in fig. 2(a), (b) and fig. 3(a), (b) for $q = 8$ and $q = \infty$, respectively. Nevertheless one should stress that a causal relation between the existence of GNF in the ordered phase and the existence of micro-phase separation in the coexistence phase, as conjectured in [11], is still hypothetical and remains an interesting open question. A comparison between fig. 5(a) and fig. 5(b) clearly reveals that GNF correspond to giant magnetization fluctuations or phase fluctuations which physically signifies weaker phase-ordering, and uniform number fluctuations correspond to smaller magnetization fluctuations which physically signifies stronger phase-ordering.

Table 1: Number fluctuation exponents ξ_n and magnetization fluctuation exponent ξ_m for several values of q, reported from fig. 5. The typical error on the fluctuation exponents is 0.01.

q	4	5	6	7	8	16	∞
ξ_n	1.04	1.08	1.36	1.56	1.62	1.62	1.65
ξ_m	1.06	1.09	1.37	1.57	1.63	1.62	1.65

The finite size effect on the number fluctuations for $q = 7$ is shown in fig. 5(c) where the data can be fitted to two different power-law regimes (consider the largest system size $L = 800$) and one can extract: i) an exponent of 1.56 in the interval $[10^2, 10^3]$ and ii) an exponent of 1.17 in the interval $[10^4, 10^5]$. These exponents along with the exponents tabulated in table 1 have been obtained by fitting the data to a power-law and since what one obtains depends on the x-range to which one restricts the fits, we have a look at the log-log slope or the corresponding effective exponent $\xi^{\rm eff} = {\rm d}[\ln(\Delta n^2)]/{\rm d}[\ln\langle n\rangle]$ plotted in fig. 5(d) (see the SM for the effective exponents corresponding to fig. 5(a), (b)). The plot shows a "plateau" around the first exponent $\xi \simeq 1.56$ but we observe no such "plateau" around the second exponent $\xi \simeq 1.17$. Therefore, on the basis of our data, even for the largest system size, one cannot predict an asymptotic value of the effective exponent which might suggests a crossover from giant to conventional number fluctuations. Note that $\xi^{\rm eff}$ must decrease with increasing $\langle n\rangle$ when $\langle n\rangle$ approaches the total number of particles in the system and becomes smaller than 1 due to the finite-size cut-off at $\langle n\rangle = N = \rho_0 L^2$, where Δn^2 vanishes.

Hydrodynamic description. – Next, we derive the main equations for the hydrodynamic continuum theory. From the microscopic hopping and flipping rates of the q-state ACM, we derive the master equation for the probability density function $n(\mathbf{x}, \theta; t)$ for a particle to be at the position $\mathbf{x}$ and in the spin-state θ at the time (see the SM). We only keep the first-order terms in the $|\mathbf{m}_i| \ll \rho_i$ expansion in the flipping rate (2). In the large system size limit $L \gg 1$, the hydrodynamic equation can be derived for the density $\rho(\mathbf{x}; t) = \int {\rm d}\theta n(\mathbf{x}, \theta; t)$ and the magnetization $\mathbf{m}(\mathbf{x}; t) = \int {\rm d}\theta \mathbf{e}_\theta n(\mathbf{x}, \theta; t)$. Assuming the magnetization is a Gaussian variable with variance proportional to ρ^ξ, as shown in fig. 5, we obtain the equations (see the SM):

$$\partial_t \rho = D_0 \nabla^2 \rho + \frac{v}{4}\nabla \cdot (\nabla \cdot Q) - v\nabla \cdot \mathbf{m}, \tag{3}$$

$$\partial_t \mathbf{m} = D_0 \nabla^2 \mathbf{m} + \frac{v}{8} \begin{pmatrix} \partial_{xx} - \partial_{yy} & 2\partial_{xy} \\ 2\partial_{xy} & -\partial_{xx} + \partial_{yy} \end{pmatrix} \mathbf{m} \\ -\frac{v}{2} (\nabla \rho + \nabla \cdot Q) + \gamma_0 \left[\beta J - 1 - r\rho^\alpha - \kappa \frac{\mathbf{m}^2}{\rho^2} \right] \mathbf{m}, \tag{4}$$

with the diffusion constant $D_0 = \overline{D}/4$, the self-propulsion velocity $v = \overline{D}\bar{\varepsilon}$, the ferromagnetic interaction strength $\gamma_0 = q\gamma/(q-1)$, $\kappa = (\beta J)^2(7 - 3\beta J)/8$, $\alpha = \xi - 2$, and the nematic tensor

$$Q = \frac{\beta J}{2\rho} \begin{pmatrix} m_x^2 - m_y^2 & 2m_x m_y \\ 2m_x m_y & -m_x^2 + m_y^2 \end{pmatrix}. \tag{5}$$

Note that, for $r = 0$, the simple mean-field theory can be recovered by neglecting the number and magnetization fluctuations. As shown in previous studies for the AIM and the APM [12,13], these mean-field equations do not predict stable phase-separated profiles and will only give the trivial homogeneous solution. We note that eqs. (3), (4) allow two homogeneous solutions with $\rho = \rho_0$ corresponding to the gas phase: $\mathbf{m} = \mathbf{0}$, and the polar liquid phase: $\mathbf{m}^2 = \rho_0^2(\beta J - 1 - r\rho_0^\alpha)/\kappa$. The order-disorder transition at $\bar{\varepsilon} = 0$ occurs at a density $\rho_* = [(\beta J - 1)/r]^{1/\alpha}$.

Equations (3) and (4) are equivalent to the hydrodynamic equations derived for the VM [11,19], although the second term of the right-hand side of both equations is absent due to the biased diffusion present in the model. Applying the conclusions made in ref. [11] to our hydrodynamic equations, we are not able to conclude when a macrophase or a microphase separation is observed in the coexistence phase. Adding a zero-mean vectorial Gaussian white noise of variance $\rho^\alpha(r - \kappa\mathbf{m}^2/\rho^\xi)$ to eq. (4) would be a possibility to scrutinize the stability of a macrophase or a microphase separation in the coexistence phase, as demonstrated for the VM in [11]. Moreover, the study of the existence of reorientation transition is feasible with eqs. (3) and (4), as already done for the APM [13].

Conclusion. – The nature of the flocking transition in the q-state ACM and the AXYM is a liquid-gas phase transition for all values of the number of states q, similar to the VM [2,11], the AIM [12] and the APM [5,13], with a coexistence phase delimiting the gas and liquid homogeneous phases for $\bar{\varepsilon} > 0$. The coexistence phase shows a macrophase separation for small directions or q-values as in the AIM [12], the APM [5,13] and microphase separation for large q values as in the VM. Longitudinally moving bands exist only when the coexistence phase is macrophase-separated, which implies that a re-orientation transition as in the APM [13] is absent for the ACM with large number of states and thus also for the AXYM, as it is for the VM. These results are supported by the number and magnetization fluctuations. Giant fluctuations observed for large q-values do not allow bulk phase separation and break large liquid domains into narrow periodic traveling bands and also restrict those bands from further coarsening, resulting in microphase separation.

Hence the discretization of the directions of motion in the VM as in the ACM will not change the characteristics of the VM flocking transition as long as the number of directions is sufficiently large. The main difference between the ACM and VM arises at zero-activity limit $\bar{\varepsilon} = 0$ where the particles in the ACM can still diffuse whereas in the VM they are immobile. For a smaller number of directions, macrophase separation and a re-orientation transition occurs. The hydrodynamic description that we derived for the q-state ACM is compatible with the hydrodynamic description for the VM presented in refs. [11,19], but is inconclusive regarding the stability of macrophase or microphase separation.

Experimental realizations of various flocking models are manifold [20] and the small-q variant of the ACM (and APM) has been used to understand pattern formation observed in experiments with motility assays [21]. For experimental systems with a large number of motility directions, the q-state ACM and the AXYM could also be a very good candidate where larger direction changes are penalized by smaller transition probabilities and a biased hopping can always be performed along the direction of motion of the particle.

When this work was finalized we became aware of a related study [22] considering a version of the ACM/AXYM that differs in various important aspects from ours: in the model used in [22] 1) particles live on a square lattice and hence can only move in four different directions, 2) spin flips (clock changes) can only happen to the previous or next hour, 3) the hopping rules are defined differently and are 4) projected onto the four lattice directions, which is not fully commensurate with the spin anisotropy, and 5) the hydrodynamic theory is one for XY spins in an anisotropy potential producing a term stabilizing LRO for all finite q-values, which is absent in our theory. For such a model an asymptotic macrophase separation and the absence of a re-orientation transition for all $q < \infty$ is predicted in [22]. The latter is a consequence of the different hopping rules [13], but to numerically prove the existence or absence of an asymptotic cross-over from micro- to macrophase separation for higher q-values one would have to consider much larger system sizes than those considered in [22] and by us and this should be clarified in a future work.

Also, an interesting problem to investigate would be the relation between the presence of GNF in the liquid phase, the nature of the coexistence phase (micro- or macrophase separation) and the pinned property of the spin, equivalent to a LRO or QLRO phase as a function of various control parameters.

* * *

This work was performed with financial support from the German Research Foundation (DFG) within the Collaborative Research Center SFB 1027. We want to thank Prof. Raja Paul for valuable discussions and for careful

reading of the manuscript. SC and MM have contributed equally to the manuscript.

Data availablity statement: All data that support the findings of this study are included within the article (and any supplementary files).

REFERENCES

[1] Shaebani M. R., Wysocki A., Winkler R. G., Gompper G. and Rieger H., *Nat. Rev. Phys.*, **2** (2020) 181.

[2] Vicsek T., Czirók A., Ben-Jacob E., Cohen I. and Shochet O., *Phys. Rev. Lett.*, **75** (1995) 1226.

[3] Aldana M., Dossetti V., Huepe C., Kenkre V. M. and Larralde H., *Phys. Rev. Lett.*, **98** (2007) 095702.

[4] Peruani F. and Aranson I. S., *Phys. Rev. Lett.*, **120** (2018) 238101.

[5] Peruani F., Klauss T., Deutsch A. and Voss-Boehme A., *Phys. Rev. Lett.*, **106** (2011) 128101.

[6] Chaté H., Ginelli F., Grégoire G. and Raynaud F., *Phys. Rev. E*, **77** (2008) 046113.

[7] Ginelli F. and Chaté H., *Phys. Rev. Lett.*, **105** (2010) 168103.

[8] Chaté H., Ginelli F., Grégoire G., Peruani F. and Raynaud F., *Eur. Phys. J. B*, **64** (2008) 451.

[9] Chaté H., Ginelli F. and Montagne R., *Phys. Rev. Lett.*, **96** (2006) 180602.

[10] Mahault B., Jiang X.-C., Bertin E., Ma A.-Q., Patelli A., Shi X.-Q. and Chaté H., *Phys. Rev. Lett.*, **120** (2018) 258002.

[11] Solon A. P., Chaté H. and Tailleur J., *Phys. Rev. Lett.*, **114** (2015) 068101; Solon A. P., Caussin J. B., Bartolo D., Chaté H. and Tailleur J., *Phys. Rev. E*, **92** (2015) 062111.

[12] Solon A. P. and Tailleur J., *Phys. Rev. Lett.*, **111** (2013) 078101; *Phys. Rev. E*, **92** (2015) 042119.

[13] Chatterjee S., Mangeat M., Paul R. and Rieger H., *EPL*, **130** (2020) 66001; Mangeat M., Chatterjee S., Paul R. and Rieger H., *Phys. Rev. E*, **102** (2020) 042601.

[14] José J. V., Kadanoff L. P., Kirkpatrick S. and Nelson D. R., *Phys. Rev. B*, **16** (1977) 1217; Cardy J. L., *J. Phys. A*, **13** (1980) 1507; Challa M. S. S. and Landau D. P., *Phys. Rev. B*, **33** (1986) 437; Baek S. K., Minnhagen P. and Kim B. J., *Phys. Rev. E*, **80** (2009) 060101(R).

[15] Kosterlitz J. M. and Thouless D. J., *J. Phys. C*, **6** (1973) 1181; Kosterlitz J. M., *J. Phys. C*, **7** (1974) 1046.

[16] Chatterjee S., Puri S. and Paul R., *Phys. Rev. E*, **98** (2018) 032109; Li Z.-Q., Yang L.-P., Xie Z.-Y., Tu H.-H., Liao H.-J. and Xiang T., *Phys. Rev. E*, **101** (2020) 060105.

[17] Woo C., Rieger H. and Noh J. D., *Suppression of discontinuous phase transitions by particle diffusion*, arXiv:2202.13895 (2022).

[18] Großmann R., Peruani F. and Bär M., *Phys. Rev. E*, **93** (2016) 040102(R).

[19] Toner J. and Tu Y., *Phys. Rev. Lett.*, **75** (1995) 4326; *Phys. Rev. E*, **58** (1998) 4828.

[20] Marchetti M. C., Joanny J. F., Ramaswamy S., Liverpool T. B., Prost J., Rao M. and Simha R. A., *Rev. Mod. Phys.*, **85** (2013) 1143.

[21] Schaller V., Weber C., Semmrich C., Frey E. and Bausch A. R., *Nature (London)*, **467** (2010) 73.

[22] Solon A., Chaté H., Toner J. and Tailleur J., *Susceptibility of Polar Flocks to Spatial Anisotropy*, arXiv:2201.00704v2 (2022).